

Nuclear envelope breakdown in starfish oocytes proceeds by partial NPC disassembly followed by a rapidly spreading fenestration of nuclear membranes

Péter Lénárt,¹ Gwénaél Rabut,¹ Nathalie Daigle,¹ Arthur R. Hand,² Mark Terasaki,^{2,3} and Jan Ellenberg¹

¹Gene Expression and Cell Biology/Biophysics Programmes, European Molecular Biology Laboratory (EMBL), D-69117 Heidelberg, Germany

²University of Connecticut Health Center, Farmington, CT 06030

³Marine Biological Laboratory, Woods Hole, MA 02543

Breakdown of the nuclear envelope (NE) was analyzed in live starfish oocytes using a size series of fluorescently labeled dextrans, membrane dyes, and GFP-tagged proteins of the nuclear pore complex (NPC) and the nuclear lamina. Permeabilization of the nucleus occurred in two sequential phases. In phase I the NE became increasingly permeable for molecules up to ~40 nm in diameter, concurrent with a loss of peripheral nuclear pore components over a time course of 10 min. The NE remained intact on the ultrastructural level during this time. In phase II the NE was completely permeabilized within 35 s. This rapid

permeabilization spread as a wave from one epicenter on the animal half across the nuclear surface and allowed free diffusion of particles up to ~100 nm in diameter into the nucleus. While the lamina and nuclear membranes appeared intact at the light microscopic level, a fenestration of the NE was clearly visible by electron microscopy in phase II. We conclude that NE breakdown in starfish oocytes is triggered by slow sequential disassembly of the NPCs followed by a rapidly spreading fenestration of the NE caused by the removal of nuclear pores from nuclear membranes still attached to the lamina.

Introduction

The stable structure of the nuclear envelope (NE)* (Gerace and Burke, 1988) that allows eukaryotes a sophisticated control of gene expression largely complicates cell division. In multicellular eukaryotes, microtubules are assembled in the cytoplasm and thus have to penetrate the NE to access chromosomes and form the mitotic spindle. NE breakdown (NEBD) is therefore an essential step of cell division that commits a cell to M-phase. It is clear that NEBD involves the disassembly and dispersal of all major elements of the NE, but the mechanism of NEBD is still far from understood.

The NE consists of two concentric membranes joined at nuclear pore complexes (NPCs) (Gerace and Burke, 1988; Allen et al., 2000). NPCs are large assemblies of ~30 different proteins termed nucleoporins (Rout et al., 2000; Cronshaw et al., 2002), which form aqueous channels that span both nuclear membranes. They allow selective traffic between nucleus and cytoplasm for particles up to ~40 nm in diameter (Görlich and Kutay, 1999; Pante and Kann, 2002) and impose a barrier to free diffusion for particles larger than ~10 nm (~50-kD proteins) (Paine et al., 1975; Keminer and Peters, 1999). The core of the NPC, the spoke ring complex, is embedded in the nuclear membranes. From its outer rim emanate eight cytoplasmic and nuclear filaments, the latter joined by a distal ring in the nuclear basket (Pante and Aebi, 1996; Allen et al., 2000). Translocation of macromolecules across the NE occurs through the center of the spoke ring, which by EM appears as a channel with ~45 nm inner diameter (Hinshaw et al., 1992; Akey and Radermacher, 1993). In metazoa, the NE is additionally stabilized by the nuclear lamina, a tight mesh of intermediate filaments underlying the inner membrane (Gruenbaum et al., 2000). The lamina is connected to both NPCs and the inner nuclear

The online version of this paper contains supplemental material.

Address correspondence to Jan Ellenberg, Gene Expression and Cell Biology/Biophysics Programmes, European Molecular Biology Laboratory (EMBL), Meyerhofstrasse 1, D-69117 Heidelberg, Germany. Tel.: (49) 6221-387-328. Fax: (49) 6221-387-518. E-mail: jan.ellenberg@embl-heidelberg.de

*Abbreviations used in this paper: INM, inner nuclear membrane; MBP, maltose binding protein; MPF, maturation promoting factor; MW, molecular weight; NE, nuclear envelope; NEBD, nuclear envelope breakdown; NPC, nuclear pore complex.

Key words: meiosis; oocyte maturation; nuclear envelope; nuclear envelope breakdown; starfish oocyte

membrane (INM) and forms the backbone of an exceptionally stable network of protein–protein interactions at the nuclear periphery (for review see Burke and Ellenberg, 2002; Burke and Stewart, 2002).

The transition from interphase to M-phase is characterized by the activation of the key mitotic regulator MPF (maturation promoting factor), which consists of cdc2 kinase in complex with cyclin B (Kishimoto, 1999). MPF is a critical factor in promoting NEBD by phosphorylating numerous proteins of the NE including lamins, INM proteins, and nucleoporins (for review see Worman and Courvalin, 2000; Burke and Ellenberg, 2002). Although phosphorylation has been shown to cause depolymerization and dispersal of lamins (Gerace and Blobel, 1980; Nigg, 1992), its effect on nucleoporins and INM proteins is much less clear. In addition, it is likely that other kinases besides MPF are required for NEBD. Active MPF injected into interphase cells is not sufficient to induce complete NEBD (Draviam et al., 2001) and lamin depolymerization in zebrafish requires phosphorylation by both protein kinase C and MPF (Collas, 1999).

Lamin depolymerization by phosphorylation and the fact that membrane vesicles from *Xenopus* egg extracts can assemble NEs around chromatin in vitro (Vigers and Lohka, 1991) led to the model that disassembly of the lamina is a prerequisite for NEBD, which would proceed by vesicularization of nuclear membranes (Marshall and Wilson, 1997). Recent observations in living cells have challenged this model. First, no traces of vesicularization were found in vivo and nuclear membrane proteins freely diffused in the ER of mitotic cells (Ellenberg et al., 1997; Yang et al., 1997; Daigle et al., 2001). Second, lamin depolymerization is a late event in NEBD that is only completed long after the disruption of the nucleocytoplasmic barrier (Beaudouin et al., 2002). What triggers NEBD therefore remained an open question. Currently, there is evidence for two different but not mutually exclusive mechanisms. In somatic mammalian cells, mechanical forces generated by interactions of the mitotic spindle with the NE have been shown to literally tear open the nuclear lamina in a dynein dependent process (Beaudouin et al., 2002; Salina et al., 2002). This process facilitates NEBD, but is not essential, as NEBD can occur in the absence of microtubules (Beaudouin et al., 2002; Salina et al., 2002). In *Drosophila* embryos and starfish oocytes in-

direct evidence points to NPC disassembly as the earliest event in NEBD. Electron microscopy of nuclei in rapidly dividing syncytial *Drosophila* embryos showed NPCs lacking cytoplasmic fibrils in prophase when nuclear membranes are still intact (Kiseleva et al., 2001). In maturing starfish oocytes, imaging nuclear entry of a large fluorescently labeled dextran was used for the first time to characterize NE permeabilization in intact cells (Terasaki, 1994). Subsequent analysis of the shape and kinetics of the dextran entry led to the hypothesis that during maturation, NPCs would initially become leaky in intact nuclear membranes, followed by a spreading disruption from the animal pole that would result in NEBD (Terasaki et al., 2001).

In this study, we tested the different models for NEBD in starfish oocytes. Starfish oocytes are an ideal system to study G2/M transition in vivo. The cells are optically clear, have a large nucleus and develop autonomously in seawater, optimal for confocal microscopy. Purified proteins and macromolecules can be introduced into the oocytes quantitatively by microinjection and the cells also support the expression of GFP fusion proteins from recombinant mRNAs. Furthermore, maturation (meiosis reentry) of the G2/prophase arrested oocytes can be triggered simply and reliably by addition of the maturation hormone 1-methyladenine, which will lead to NEBD within 20 min.

We have exploited this system for a detailed characterization of NEBD in intact cells by quantitative confocal time-lapse microscopy as well as EM. We show that NEBD proceeds in two clearly defined phases of nuclear permeabilization. During the first phase, peripheral nucleoporins were sequentially released from the nuclear rim, evidence for the stepwise NPC disassembly. Nucleoporin release coincided with an increasing permeability for macromolecules up to ~40 nm diameter and a leakage of nuclear import substrates, while the NE remained intact at the ultrastructural level at this time. In the second phase, a wave of permeabilization rapidly spread across the nuclear surface. Passage of the wave allowed entry of macromolecules as large as 100 nm in diameter into the nucleus. Although the lamina and nuclear membranes appeared intact by light microscopy at this time, at the EM level the NE was fenestrated by ~200 nm gaps. We propose that the second phase proceeds by a spreading fenestration

Table 1. Properties of the fluorescent dextrans and proteins

	Molecular weight	D _{water}	Diameter ^a	Pore diameter to allow one molecule s ⁻¹ flux ^a
	kD	μm ² /s	nm	nm
Dextrans	500	7.1	93	98
	160	12.5	53	57
	90	16.4	40	43
	70	18.2	36	39
	25	32.4	20	22
	10	62.4	10.6	12
GFP	27	90 ^b	2.4 × 4.2 ^c	4.7
MBP	42	60	3 × 4 × 6.5 ^d	6.2

^aFor description of the calculations see Online supplemental material.

^bKohler et al., 2000.

^cDimensions of the crystal structure (Brejc et al., 1997).

^dDimensions of the crystal structure (Spurlino et al., 1991).

mechanism that is caused by the removal of the remaining core of NPCs from the NE.

Results

Probing NE permeability with fluorescent dextrans in immature oocytes

To measure the permeability of the intact NE in immature oocytes, we injected different sizes of fluorescently labeled dextrans (Table I; see also Online supplemental material available at <http://www.jcb.org/cgi/content/full/jcb.200211076/DC1>) into the cytoplasm and monitored their ability to enter the nucleus by measuring the increase

of mean fluorescence intensity in the nuclear region over time. A 10-kD dextran entered the nucleus of immature oocytes rapidly by passive diffusion and equilibrated between nucleus and cytoplasm in ~ 30 min (Fig. 1, A and C). The two times higher fluorescence intensity in the nucleus as compared with the cytoplasm after equilibration is due to yolk platelets that occupy $\sim 50\%$ of the cytoplasmic volume, except for a small rim of yolk-free cytosol directly adjacent to the NE (Fig. 1 D). Dextrans with larger molecular weights (MW), such as 25 kD, were excluded during this time (Fig. 1, B and C), and even after 2 wk $<50\%$ had entered the nucleus. Fractions above 25 kD did not enter the nucleus at all even during such prolonged periods (unpublished data). Thus, in immature oocytes, dextrans with

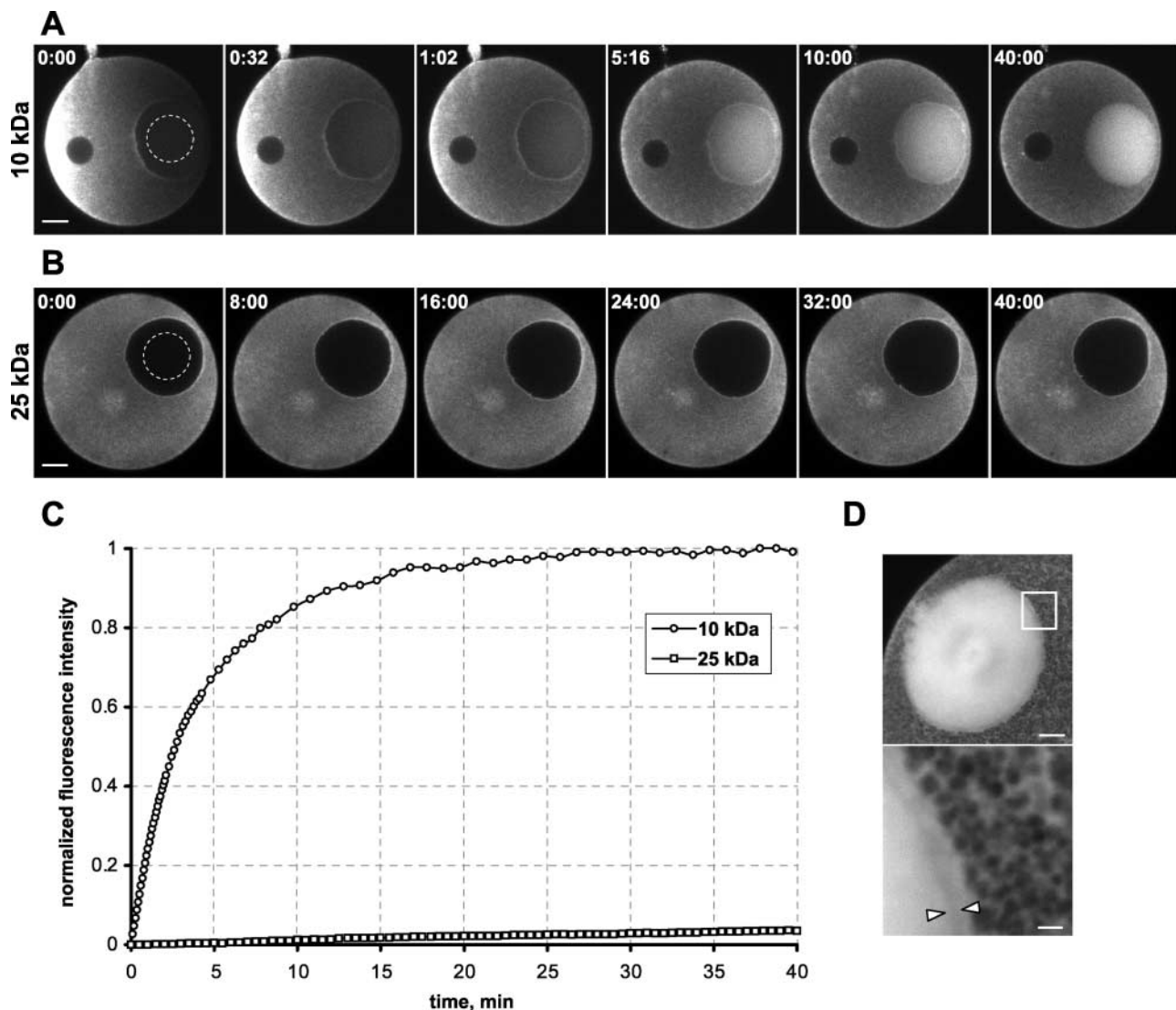


Figure 1. NE permeability in immature oocytes. (A) Immature starfish oocyte injected with Alexa 488 10-kD dextran and imaged immediately after injection. Dextran diffuses from the vegetal pole through the cytoplasm and simultaneously fills the nucleus. Note accumulation of dextran adjacent to the nuclear rim at early times, indicating that nuclear entry is slower than diffusion. Selected frames are shown, for complete sequence see Video 1, available at <http://www.jcb.org/cgi/content/full/jcb.200211076/DC1>. Bar, 25 μ m. Time, mm:ss. (B) Time series of an immature starfish oocyte injected with Alexa 488 25-kD dextran. Scale and time as in A. (C) Quantitation of mean nuclear (dashed lines in A and B) fluorescence over time of the sequences shown in A and B. Intensities were normalized from initial to final values (A), or from minimum to two times the average cytoplasmic values (B). (D) High-resolution confocal image of a 10-kD dextran-injected oocyte after equilibration. Cytoplasm is filled with yolk platelets, resulting in an apparent 50% lower concentration. High magnification inset (bottom) shows single platelets and a yolk-free zone adjacent to the NE (arrowheads). Bars: 10 (μ m) (top) and 2 μ m (bottom).

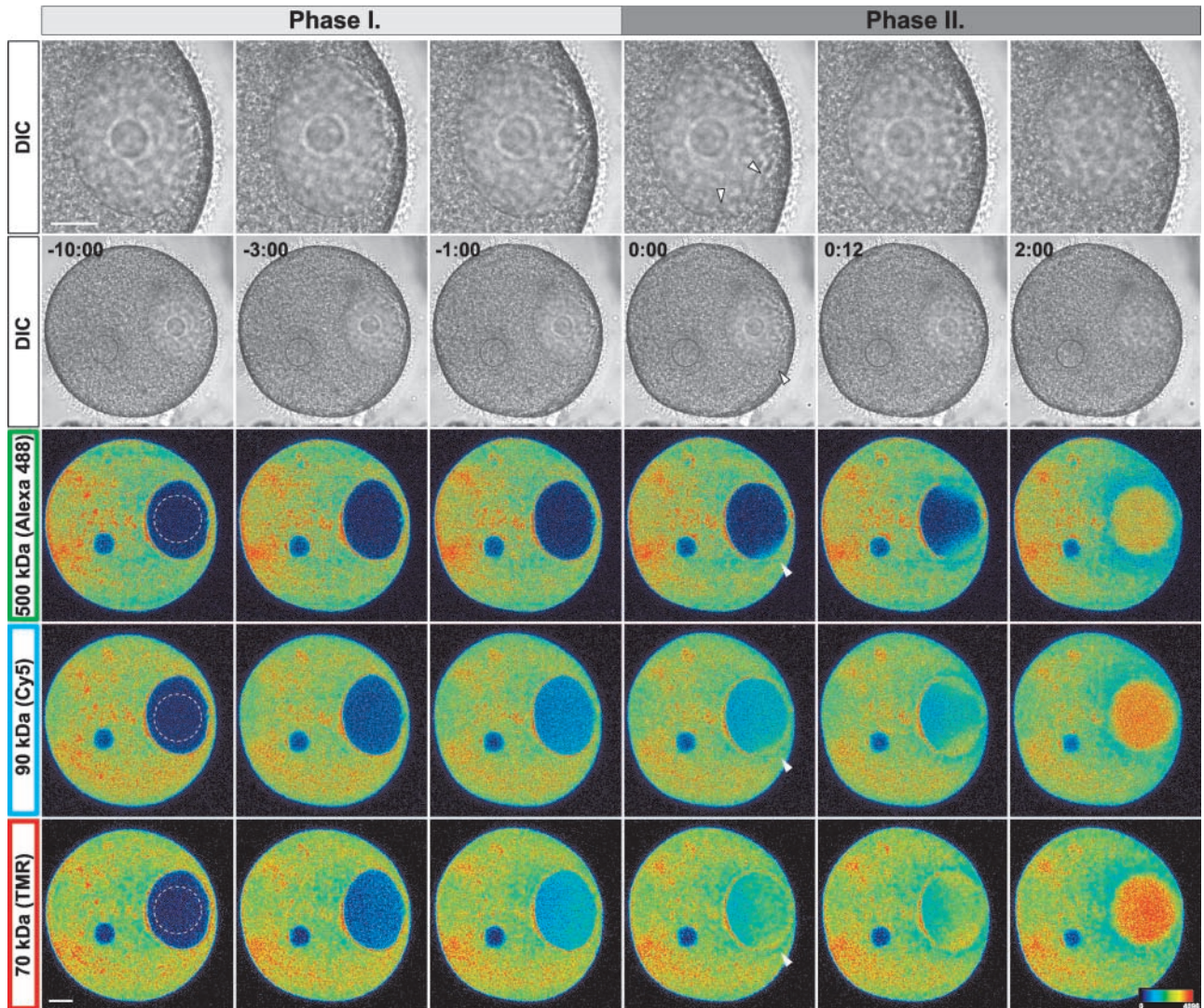
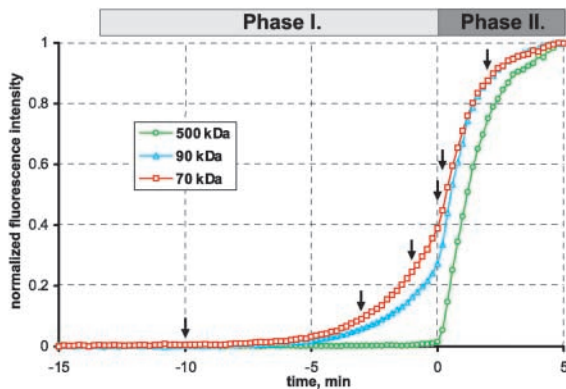
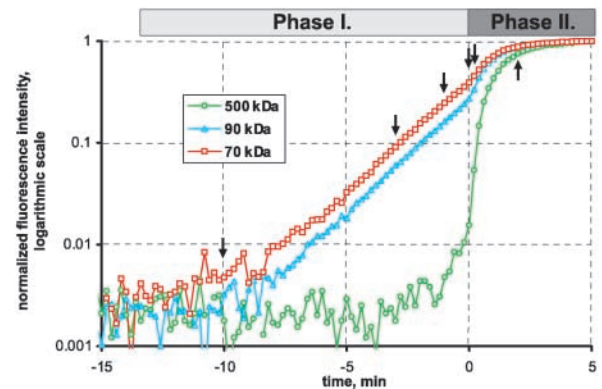
A**B** Entry kinetics**C** Entry kinetics, logarithmic scale

Figure 2. Two phases of dextran entry during NEBD. (A) Oocyte coinjected with 500, 90, and 70 kD dextrans labeled with Alexa 488, Cy5, and TMR, respectively. Arrowheads mark the start of complete permeabilization also visible by DIC. At 2:00 the 500-kD dextran is equilibrated only to 90% due to its slow diffusion. Small dark circle in the cytoplasm is an oil drop from the injection. Fluorescence images are pseudo colored for easier comparison. Selected frames are shown, for complete sequence see Video 2, available at <http://www.jcb.org/cgi/content/full/jcb.200211076/DC1>. Bar, 25 μ m. Time mm:ss, 0:00 = start of 500-kD dextran entry. (B) Quantitation of mean nuclear (dashed lines in A) fluorescence of time series shown in A, normalized from minimum to maximum values. Arrows mark time points shown in A. (C) As in B, plotted semilogarithmically to compare entry rates.

diameters of ~ 10 nm (10 kD) were able to pass through intact nuclear pores, whereas NPCs efficiently excluded larger molecules from the nucleus. Dextran of 25 kD or larger (≥ 20 nm in diameter) were only able to enter the nucleoplasm during NEBD, at oocyte maturation (Terasaki, 1994; Fig. 2 A).

NEBD proceeds in two phases in maturing oocytes

Depending on their size, dextran fractions showed differential behavior during NEBD induced by oocyte maturation. By using combinations of different fluorophores we could monitor three different sizes of dextran simultaneously in the same cell and observe changes in the NE by differential interference contrast (DIC) (Fig. 2 A).

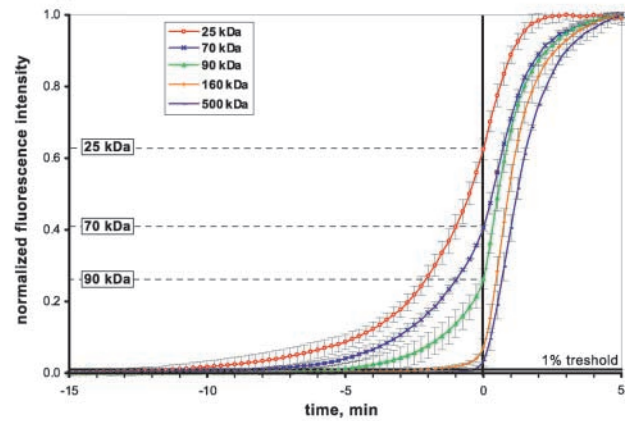
A 500-kD dextran entered the nucleus as a rapid wave ~ 20 min after maturation hormone addition (Fig. 2, A and B, 500 kD). The wave passed through the entire nucleus within only 30 s. The start of the wave corresponded precisely to the point when the first change at the boundary between the cytoplasm and nucleus could be observed by transmitted light microscopy (Fig. 2 A, DIC, see also Video 2, available at <http://www.jcb.org/cgi/content/full/jcb.200211076/DC1>). The entry of a 500-kD dextran thus coincided with the classical definition for the onset of NEBD and will be used as a reference time point for NEBD in this study. Dextran smaller than 160 kD but larger than 10 kD started to enter the nucleus gradually and homogeneously ~ 10 min before the start of the wave (Fig. 2 A, 70 and 90 kD, and Fig. 2 B; see also Video 2). At this time however, no changes at the nuclear rim could be detected by transmitted light (Fig. 2 A, DIC).

Thus we could define two phases of NEBD: phase I comprised gradual changes in nuclear permeability that occurred before the entry wave of large dextran, and phase II, which comprised the rapid entry wave and visible changes in the nuclear rim by transmitted light. In phase I the nucleus became accessible for small macromolecules up to 40 nm in diameter (90-kD dextran), whereas in phase II even molecules with sizes of 93 nm (500-kD dextran, the largest tested) could enter the nucleus freely (Fig. 2 B). Phase I occurred over a period of ~ 10 min, while phase II was completed in 35 s. In phase I the permeability of the NE increased slowly with single exponential kinetics (Fig. 2 C), while in phase II nucleus and cytoplasm equilibrated rapidly in a process limited by diffusion. In phase I dextran filled the nucleus homogeneously (Fig. 2 A, 70 and 90 kD). Phase II, by contrast, proceeded as an entry wave that started at a single site on the NE and then rapidly spread across the nuclear surface (Fig. 2 A, 500 kD, arrowheads).

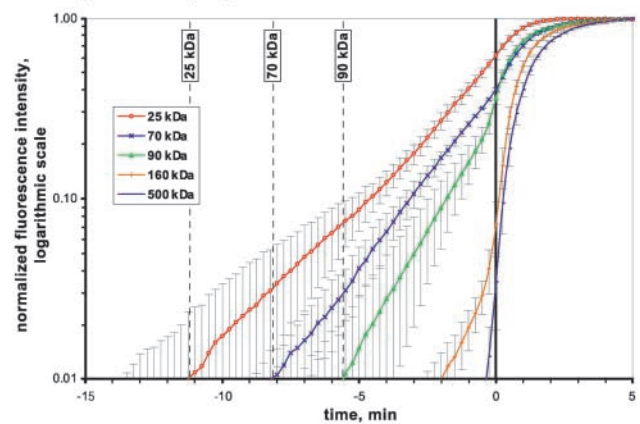
Phase I: the apparent diameter of the NPC diffusion channel increases from 12 to 40 nm

To characterize changes in NE permeability during phase I quantitatively, we used dextran fractions of 25–90 kD and compared experiments similar to the one shown in Fig. 2 A from many cells using the start of the 500-kD entry wave to align the series in time. The 25-kD dextran started to enter the nucleus at -11 min and more than 60% of the final nuclear amount had already passed the NE at the end of phase I (Fig.

A Entry kinetics



B Entry kinetics, logarithmic scale



C Rate of entry

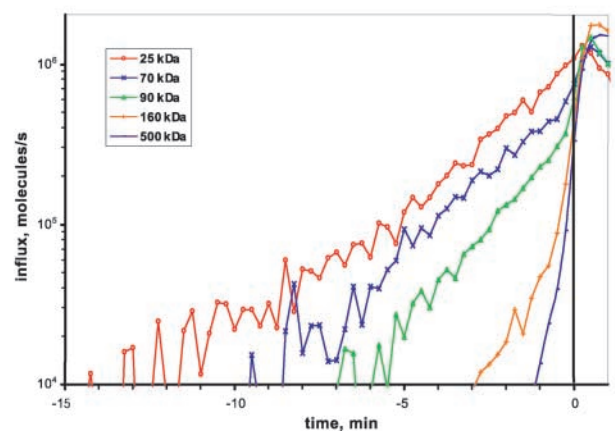


Figure 3. Sequential entry of different size dextrans during phase I of NEBD. (A) Average values and standard deviations of experiments similar to Fig. 2 B. $n = 5, 3, 9, 19,$ and 6 for the 25-, 70-, 90-, 160-, and 500-kD dextrans, respectively. (B) As in A plotted semilogarithmically to compare entry rates and the time differences of the start of entry. A 1% increase was defined as the starting point of entry (see A and Fig. 2 C). (A and B) The $<7\%$ of the 160-kD dextran that entered before phase II most likely represent the entry of the smaller molecules in the polydisperse fraction (see Discussion). (C) Entry rates of dextran molecules into the nucleus, calculated for all individual datasets shown in B and averaged (for details see Online supplemental material available at <http://www.jcb.org/cgi/content/full/jcb.200211076/DC1>).

3, A and B, $n = 5$). Larger dextran fractions of 70 and 90 kD started later, at -8 and -5.5 min and only 40% and 25% entered in phase I, respectively (Fig. 3, A and B, $n = 3$ and 9). Although the dextrans started to enter the nucleus at different times, their rates of entry were very similar as is evident from the slopes of the curves in a semilogarithmic plot (Fig. 3 B). These entry kinetics caused by maturation were clearly distinct from the slow and simultaneous entry of all dextran sizes through a single, but relatively large perforation ($\sim 1 \mu\text{m}$) produced by a microneedle in the nucleus of an immature oocyte (Fig. S1). Entry kinetics were also not a result of the polydispersity of dextran fractions, because proteins of comparable size (such as MBP; maltose binding protein) showed similar behavior to the dextrans during phase I (Fig. S2).

Thus, different sized macromolecules gained access to the nucleus sequentially, according to their diameter, but once allowed to enter their influx kinetics were governed by the same dynamic increase in permeability. These observations strongly suggested that the size exclusion limit of the NPCs continuously increases during phase I of NEBD. As the exclusion limit reached their respective size, larger and larger dextran fractions were able to enter the nucleus. Dextrans of 160 kD or larger, however, continued to be excluded in phase I.

To confirm that changes in NPC permeability could account for the observed dextran entry during phase I, we calculated the fluxes of dextrans through NPCs, assuming that all pores behave similarly. Because we injected known amounts of dextrans, changes in fluorescence intensity could be directly converted into the number of molecules entering the nucleus. Normalized to $2 \mu\text{M}$ initial cytoplasmic concentration (see Online supplemental material available at <http://www.jcb.org/cgi/content/full/jcb.200211076/DC1>), 25–90 kD dextrans reached peak fluxes of $\sim 10^6$ molecules s^{-1} at the end of phase I of NEBD (Fig. 3 C). As estimated from EM images, oocyte nuclei contain $\sim 10^6$ NPCs (Stricker and Schatten, 1989, Fig. 5 D). The fluxes thus correspond to one molecule $\text{NPC}^{-1} \text{s}^{-1}$. The flux of the 10-kD dextran, which entered through the intact NE of immature oocytes, was also very similar (Fig. 1, unpublished data). Assuming diffusion-driven flux, the diameter of an aqueous channel, which would support a flux of one molecule $\text{NPC}^{-1} \text{s}^{-1}$ for the different dextran sizes can be calculated (Table I, for details see Online supplemental material). A channel of ~ 12 nm diameter would support the 10-kD dextran flux in the intact NE, while at the end of phase I of NEBD this diameter would have to increase to 30–40 nm to support the observed flux of the 25–90-kD dextrans.

Thus, our data is consistent with the known dimensions of the NPC and suggests that NPC disassembly is responsible for the increasing permeability in phase I of NEBD. The sequential entry of molecules of increasing size could be explained by the sequential dissociation of different elements of the NPC, which would gradually increase the pore diameter. At the end of phase I only a core channel with a diameter of ~ 40 nm would remain, explaining the discrimination against molecules >40 nm in diameter at this point.

Import substrates are released from the nucleus during phase I

If the apparent diameter of the NPC diffusion pore increases from 12 to 40 nm during phase I of NEBD due to NPC dis-

assembly, we would predict defects in nucleocytoplasmic transport at this time. To test this prediction, we used well-characterized import substrates, MBP fused to an importin- β binding domain (IBB-MBP) and a transportin specific import signal (M9-MBP), both labeled with Alexa 594 (Ribbeck and Görlich, 2002; Katharina Ribbeck, personal communication). Both proteins were efficiently imported into the nucleus of starfish oocytes (unpublished data). To simultaneously follow the changes in active transport and passive diffusion we coinjected M9- or IBB-MBP with MBP (without import signal) into the nucleus of oocytes together with a cytoplasmically injected large dextran (500 kD) (Fig. 4, Videos 3, A and B, available at <http://www.jcb.org/cgi/content/full/jcb.200211076/DC1>). M9-MBP was released with kinetics strikingly similar to MBP (Fig. 4, A and B)

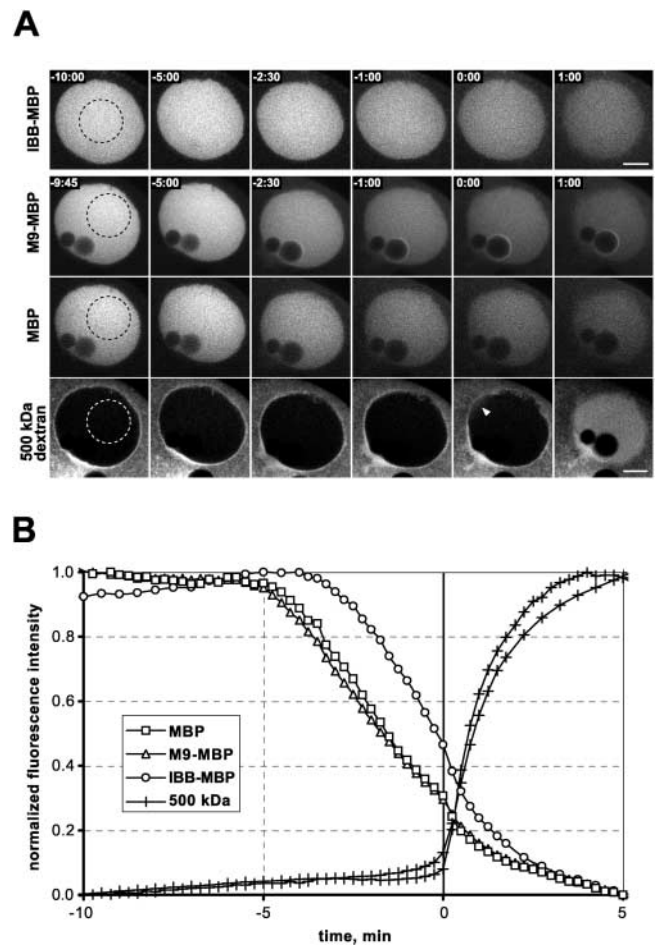


Figure 4. Import substrates are released from the nucleus during phase I of NEBD. (A) Oocytes coinjected with Alexa 594 IBB-MBP or M9-MBP and Alexa 488 MBP into the nucleus and Cy5 500-kD dextran into the cytoplasm (MBP and dextran shown only for M9-MBP). Selected frames are shown, for complete sequences see Video 3, A and B, available at <http://www.jcb.org/cgi/content/full/jcb.200211076/DC1>. Bar, 25 μm . Time, mm:ss. Arrowhead, the dextran entry wave. (B) Quantitation of mean nuclear (dashed lines in A) fluorescence intensities of the time series shown in A, normalized from minimum to maximum values. The two sequences were aligned by the 500-kD dextran entry. The slow entry of the 500-kD dextran before 0 min is due to the small hole created by the nuclear injection.

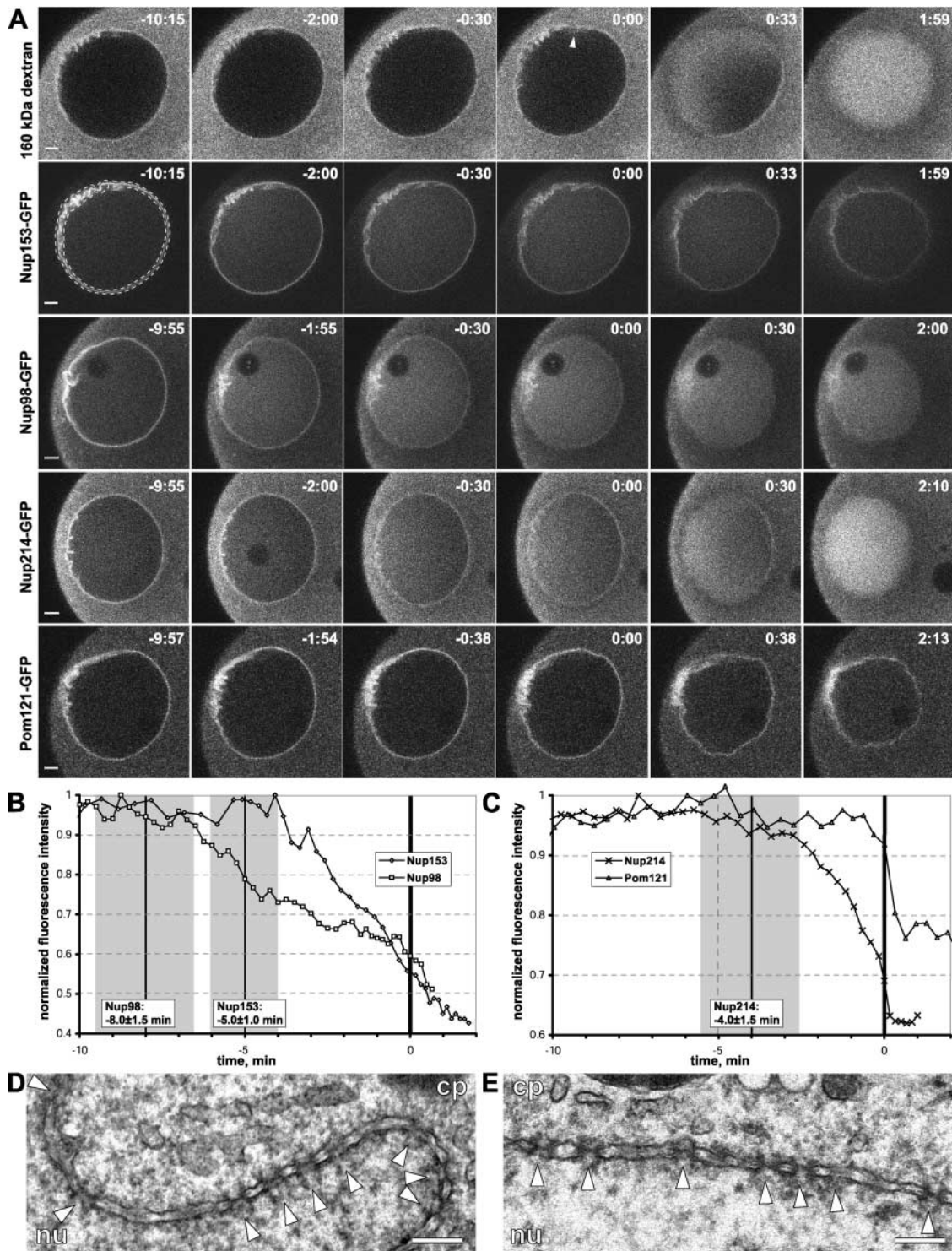


Figure 5. **Nucleoporins are released from the NE in phase I of NEBD.** (A) Maturation of oocytes expressing nucleoporin-GFP fusion proteins coinjected with TRITC 160-kD dextran (only shown for Nup153); arrowhead marks initial entry site. For some nucleoporins a nucleolar or cytoplasmic pool is present in addition to the nuclear rim, and the nucleolus becomes visible (e. g. Nup98). Selected frames are shown, for complete sequences see Videos 4, A–D, available at <http://www.jcb.org/cgi/content/full/jcb.200211076/DC1>. Bars, 10 μ m. Time, mm:ss. (B) Dissociation kinetics of Nup98 and Nup153. Quantitation of mean fluorescence intensities of the nuclear rim (dashed line in A) of the time series shown in A, normalized from background to maximum values. Vertical black lines mark average time of the start of release determined from independent experiments, gray area indicates standard deviation. (C) Dissociation kinetics of Nup214/CAN and POM121. Quantitation as in B. (D) Thin section electron micrograph of the NE of an immature oocyte. cp, cytoplasm; nu, nucleus; arrowheads, NPCs. Bar, 200 nm. (E) Thin section electron micrograph of the NE of an oocyte at the end of phase I (1–2 min before the initiation of phase II). Labeled as in D. Bar, 200 nm.

starting at -6.8 ± 1 min ($n = 11$). At the end of phase I, $>70\%$ of the proteins had been released into the cytoplasm. The release of IBB-MBP started slightly later (-3.8 ± 0.6 min, $n = 6$) and showed a different kinetics, which might be a result of the retention of IBB-MBP by binding to other nuclear factors (Fig. 4, A and B). The release of two different types of import substrates from the nucleus during phase I further suggested that NPC disassembly is responsible for the increased NE permeability in phase I and also indicates the dual role of the NPC controlling nuclear transport and passive diffusion through the NE.

Peripheral nucleoporins are released from the NE in phase I

To directly visualize changes in NPC composition we next expressed GFP-tagged mammalian nucleoporins in oocytes by injecting their mRNAs before maturation. The fusion proteins localized correctly to the NE, indicating that they were incorporated into the NPCs (Fig. 5 A). Oocytes expressing chimeric nucleoporins matured with normal kinetics and morphology and imported NLS containing import substrates indicating that the presence of heterologous proteins did not greatly interfere with nucleocytoplasmic transport (unpublished data). We estimated the expression levels of GFP-nucleoporins by comparison with oocytes injected with known amounts of recombinant GFP. For the most highly expressed nucleoporin (Nup153) we calculated ~ 2 chimeric proteins per NPC (Fig. S3) while this number was significantly lower for the other nucleoporins.

We then examined whether these proteins dissociated from the NE during phase I of NEBD by measuring their intensity on the nuclear rim during maturation. The first change observed was for two nucleoporins of the nuclear basket, Nup98 and Nup153, which started to dissociate from the NE at -8 ± 1.5 min ($n = 5$) and -5 ± 1 min ($n = 6$), respectively (Fig. 5, A and B, see also Video 4, A–D, available at <http://www.jcb.org/cgi/content/full/jcb.200211076/DC1>). At the end of the first phase $>50\%$ of the proteins were released from the NE (Fig. 5 B). A nucleoporin localized to the cytoplasmic face of the NPC, Nup214/CAN, started to dissociate at -4 ± 1.5 min ($n = 5$, Fig. 5, A and C). The remaining fraction of Nup98, Nup214, and most of Nup153 then dissociated rapidly in the second phase with the permeabilization wave (Fig. 5 A). By contrast, the transmembrane protein POM121, a stable component of the NPC core, showed no dissociation during phase I, and only a fraction ($\sim 20\%$) was released at the onset of the second phase (Fig. 5, A and C, $n = 6$). Thus, coinciding with the slow dextran entry in phase I several peripheral nucleoporins were sequentially released from NPCs, providing direct evidence for gradual NPC disassembly. POM121 remained stably associated with the NE, indicating that a residual NPC structure is still intact, consistent with the exclusion of dextrans >40 nm in phase I.

To provide further evidence that NPC disassembly is responsible for the increased permeability of the NE in phase I, we extended our observations to the ultrastructural level. Transmission EM on thin sections of resin-embedded oocytes was performed at different stages of maturation. In good agreement with the light microscopy data, on EM sec-

tions of both immature and phase I oocytes the overall NE structure showed no discontinuities other than NPCs, all with similar structure and regularly spaced every ~ 200 nm (Fig. 5, D and E). Whereas in immature oocytes cytoplasmic filaments and nuclear baskets could be distinguished in $\sim 25\%$ of the NPCs (Fig. 5 D, arrowheads), the length and number of filamentous structures detected was reduced in oocytes fixed during phase I (Fig. 5 E, arrowheads). Thus, NPCs were the only structures that connected nucleus and cytoplasm and therefore would be able to mediate entry of the 25–90-kD dextrans during phase I. The loss of peripheral filaments indicates NPC disassembly in good agreement with the observed release of the GFP-nucleoporins by light microscopy.

Phase II: a wave of breakdown across the nuclear surface

Phase II of NEBD was marked by an entry wave of even very large macromolecules into the nucleus. This wave initiated at a single location on the NE and then rapidly spread across the nuclear surface (Fig. 6 A, see also Video 5 A). The large 500-kD dextran with 93-nm diameter could freely enter the nucleus through the permeabilized regions of the NE at this time (Fig. 6, A and E). The local fluxes measured at the permeabilized areas were about five times higher than the peak flux at the end of the first phase (see Online supplemental material available at <http://www.jcb.org/cgi/content/full/jcb.200211076/DC1>) and the kinetics of phase II also fitted well to simulating free diffusion of dextran through an expanding hole into the nucleus (Terasaki et al., 2001). In this way the nucleus equilibrated with the cytoplasmic dextrans in <1 min.

To directly visualize the spreading of the permeabilization zone on the NE, we used fast three-dimensional time-lapse (4D) imaging (Gerlich et al., 2001) of the entire nucleus during oocyte maturation. Single optical sections from such datasets demonstrated that the dextran entered the nucleus rapidly over short distances at the nucleocytoplasmic boundary but diffused only slowly over long distances to the middle of the nucleus (Fig. 6 A). This behavior explained the concave shape of the wave front seen in earlier studies (Terasaki et al., 2001). Dextran entry into the nucleus was mirrored by rapid depletion from the yolk-free zone around the nucleus in the cytoplasm (Fig. 6 A, see also Fig. 1 D). Surface reconstruction of the entire 4D dataset revealed that the permeabilized areas of the NE rapidly spread from a single initiation point (Fig. 6 B, see also Video 5 B). The wave front spread with an average speed of $1\text{--}2 \mu\text{m s}^{-1}$ in all directions, finally engulfing the entire nucleus after 35 s.

Analysis of several cells showed that the site of initiation was reproducibly located on the animal hemisphere close to the equatorial region ($n = 10$) (Fig. 6, C and D) and was not found directly at the animal pole in any of our 2D or 3D time-lapse datasets ($n > 50$, unpublished data). In all cases, permeabilization initiated at a single site that could be followed by one or two secondary sites 5–20 s later. The 3D reconstructions also demonstrated that the impression of two sites of permeabilization gained from 2D sequences (e.g., on Fig. 2 A) resulted from the spreading from a single site outside the plane of observation,

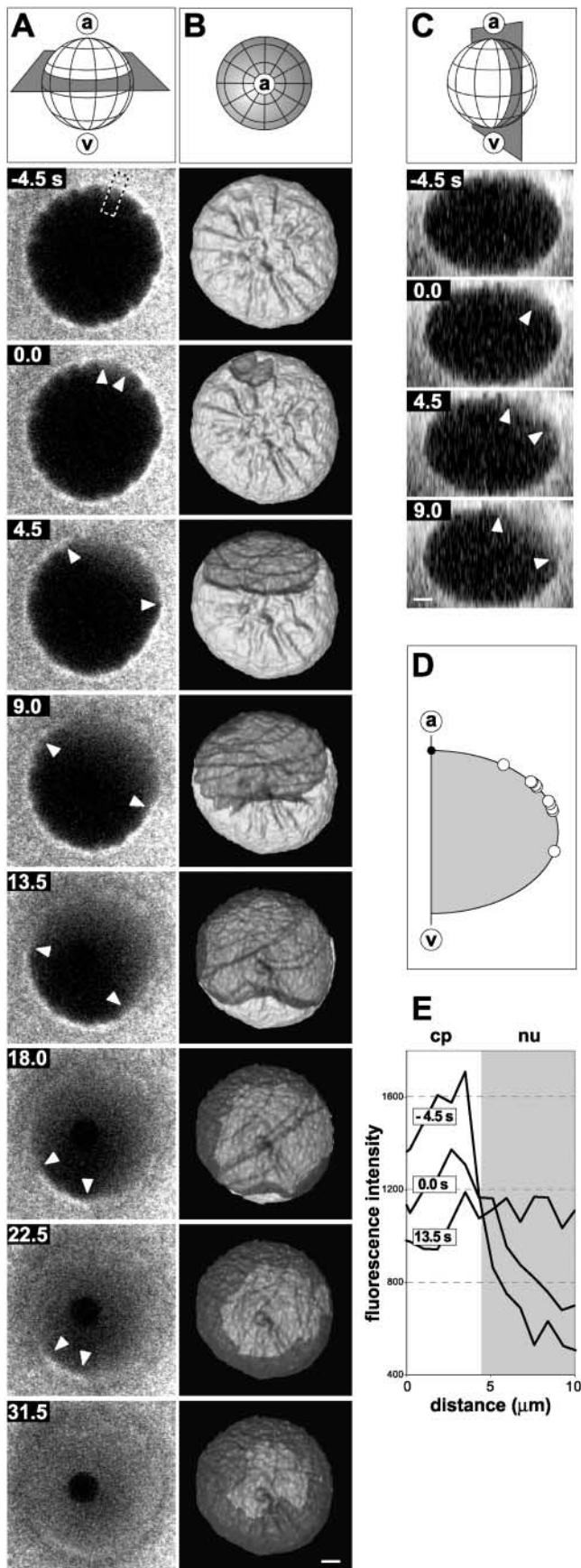


Figure 6. **Permeabilization wave of the NE during phase II of NEBD.** Oocyte injected with Alexa 488 500-kD dextran imaged in 3D over time during maturation. See also Video 5, A and B, available

which reaches the optical section at two points simultaneously (Fig. 6 B).

The lamina and nuclear membranes remain globally intact during phase II

Since peripheral nucleoporins were almost completely lost from the NE during the time in which NPC permeabilization spread over the NE (Fig. 5 A), we investigated if other NE structures such as the lamina and the nuclear membranes were also disassembled at this time. Indication that parts of the NE structure must remain intact during phase II came from the observation that a clear boundary between the cytoplasm and nucleus was observed during phase I and II of NEBD by DIC (Fig. 2 A), 500-kD dextran (Fig. 6 A), and POM121 fluorescence (Fig. 5 A). Although this boundary was completely permeable for molecules up to 93-nm diameter, it still prevented the entry of larger particles such as yolk platelets into the nucleoplasm (Fig. 7 A, DIC). Nuclear membranes and the lamina were labeled with the membrane dye DiIC₁₆ and GFP tagged lamin B, respectively, and visualized directly during NEBD together with a 500-kD dextran in the same cell (Fig. 7 A, see also Video 6, available at <http://www.jcb.org/cgi/content/full/jcb.200211076/DC1>). Such time-lapse sequences ($n = 5$) showed that the dextran wave entered through the lamina and nuclear membranes that appeared intact by confocal microscopy and could thus not contain gaps $>1 \mu\text{m}$ (Fig. 7 A, 0:00). Indeed, on electron micrographs of oocytes fixed at the beginning of phase II, gaps with a size of 100–200 nm could be seen (Fig. 7, B and C), which would account for the rapid diffusion of the largest dextran molecules, but still escape the resolution of the confocal microscope. At this stage the NE consisted of membrane elements of 1–2 μm in length containing 3–10 NPC-like structures, which appeared to be in different stages of disassembly (Fig. 7, B and C). This is consistent with our light microscopy data that all peripheral nucleoporins are released at this time while a significant fraction of POM121 fluorescence remained associated with the NE (Fig. 5, A and C). By light microscopy large discontinuities could only be detected several minutes later. These holes appeared simultaneously in the polymerized lamina and nuclear membranes that were still attached to the lamina (Fig. 7 A).

at <http://www.jcb.org/cgi/content/full/jcb.200211076/DC1>. Bars, 10 μm . (A) Selected optical slice from the 4D dataset showing initiation and spreading of the permeabilization. Arrowheads mark the boundary between permeabilized and intact NE. The nucleolus excludes the dextran and becomes visible in the last two frames. (B) Isosurface visualization of the complete 4D dataset. Intact (light gray) and permeabilized (dark gray) areas of the NE were segmented and reconstructed in 3D. (C) Animal-vegetal optical cross section of the 4D dataset shown in A and B. Permeabilization is initiated between the animal pole and equator of the nucleus (arrowheads). (D) Positions of the initial entry site from 10 experiments analyzed as in C. Distance from the animal pole normalized to the height of the nucleus is plotted on a scheme of the nuclear surface. (E) Line profiles of fluorescence intensity along the primary entry site (shown by a dashed rectangle on A) at different time points. cp, cytoplasm; nu, nucleus.

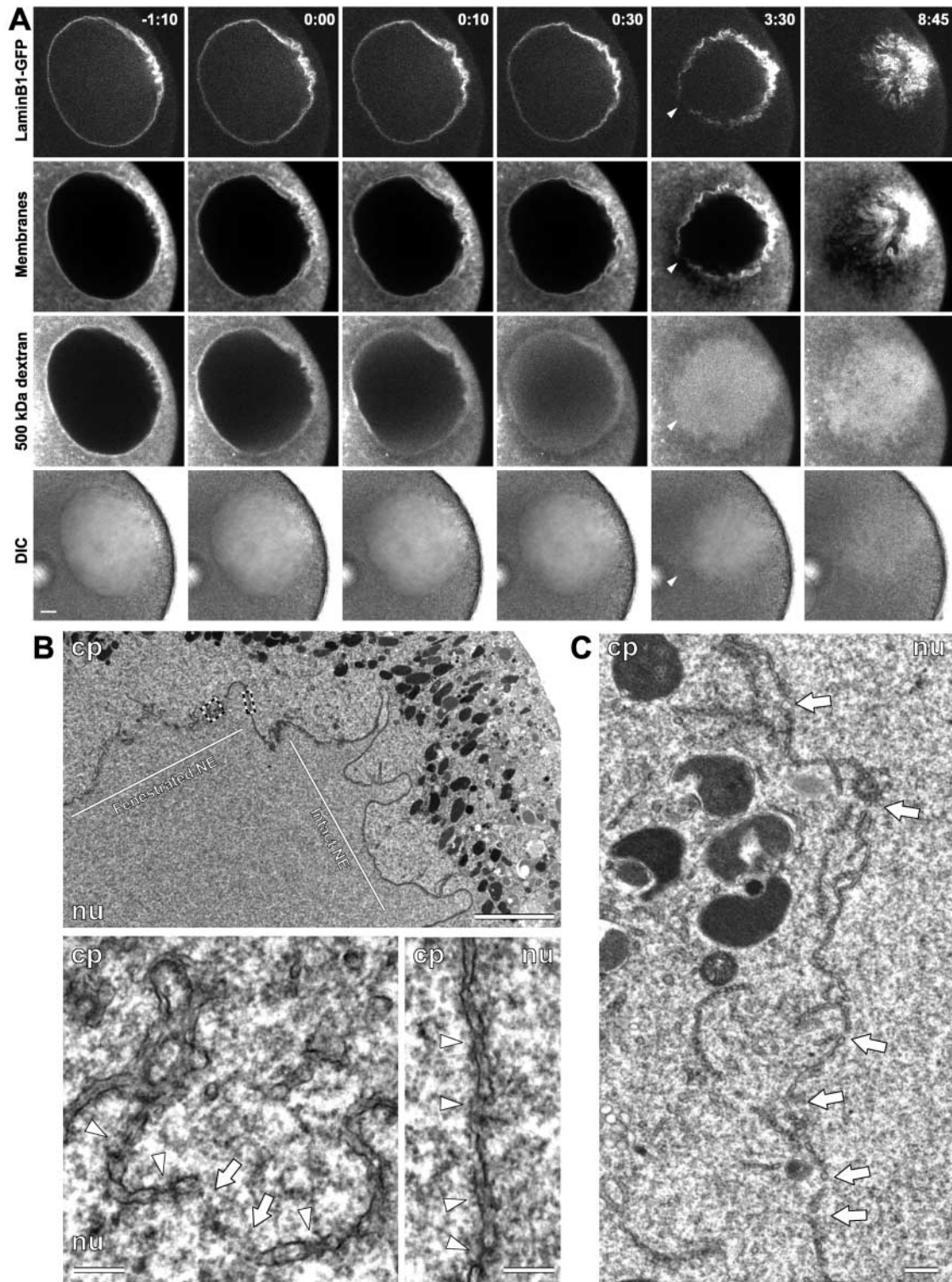


Figure 7. Fenestration of the NE in phase II. The lamina and nuclear membranes remain intact on the light microscopic level. (A) Oocyte expressing Lamin B1-GFP coinjected with the lipophilic dye DiI₁₆ and Cy5 500-kD dextran. Selected frames are shown, for complete sequence see Video 6, available at <http://www.jcb.org/cgi/content/full/jcb.200211076/DC1>. Bar, 10 μ m. Time, mm:ss, 0:00 = start of 500-kD entry. Arrowhead marks first visible gap. (B) Thin section electron micrograph of the NE of an oocyte at the initiation of phase II. cp, cytoplasm; nu, nucleus; arrowheads, disassembling NPCs; arrows, gaps on the NE. Dashed rectangles mark regions shown in the bottom panels at higher magnification. Bar, 5 μ m (top) and 200 nm (bottom). (C) Thin section electron micrograph of the NE of an oocyte during phase II, at a later stage than B. Labeled as in B. Bar, 1 μ m.

The lamina was completely solubilized >10 min after the beginning of phase II (unpublished data).

We had shown before that in cultured somatic mamma-

lian cells the permeabilization of the NE for large dextrans proceeds by microtubule-induced tearing, resulting in large holes in nuclear membranes and the nuclear lamina that are

readily visualized by confocal microscopy (Beaudouin et al., 2002). Since we did not observe such holes or dramatic nuclear deformations during permeabilization of the nucleus of starfish oocytes, we tested if NEBD in this system is facilitated by microtubules by depolymerizing them with nocodazole. Consistent with results reported in an earlier study (Stricker and Schatten, 1991), NEBD was neither blocked nor delayed by nocodazole compared with control oocytes (Fig. S4). Moreover, no difference in the speed or morphology of the spreading of the permeabilization wave was detected (Fig. S4).

Discussion

Fluorescent dextrans as probes for NE permeability

In this study, we used fluorescently labeled dextran fractions to probe permeability changes of the NE in maturing starfish oocytes. Dextran is an ideal size probe because above MW of ~ 2 kD their structure is well approximated by a random coil conformation (Luby-Phelps, 1989). For random coils an increase in MW increases the diameter but does not affect shape and surface properties (Luby-Phelps, 1989). This is essential for studies on the NE permeability, because passage through the NPC is strongly dependent on both shape and surface properties of proteins (Ribbeck and Görlich, 2001, 2002). In contrast to pure polypeptides, however, dextran fractions are polydisperse mixtures (Luby-Phelps, 1989). Our FCS measurements that we used to cali-

brate dextran sizes (see Online supplemental material available at <http://www.jcb.org/cgi/content/full/jcb.200211076/DC1>) thus provided a mean value for the size of a fraction. The spread of a fraction as estimated by gel filtration measurements is less than $\pm 50\%$ in diameter. This does not affect our conclusions about changes in NPC channel size; however, the minor pool of the 160-kD dextran fraction that entered the nucleus at the end of phase I is most likely a consequence of this polydispersity. In addition, the continuous increase in NE permeability during phase I was also observed with monodisperse proteins of comparable sizes.

NEBD starts with the gradual disassembly of peripheral nucleoporins

Phase I of NEBD lasted for ~ 10 min and was characterized by the gradual entry of macromolecules between 20 and 40 nm diameter into the nucleus. Our observations are best explained by a model in which the sequential loss of peripheral nucleoporins from NPCs continuously increases their permeability until only an “empty” core channel embedded in the otherwise intact NE is left behind (Fig. 8, A and B).

Our data provide four lines of evidence in support of this model:

(a) **Dextrans entered sequentially according to their size.** The sequential entry clearly showed that changes in NE permeability corresponded to a gradual opening rather than the instantaneous removal of the entire NPCs or larger

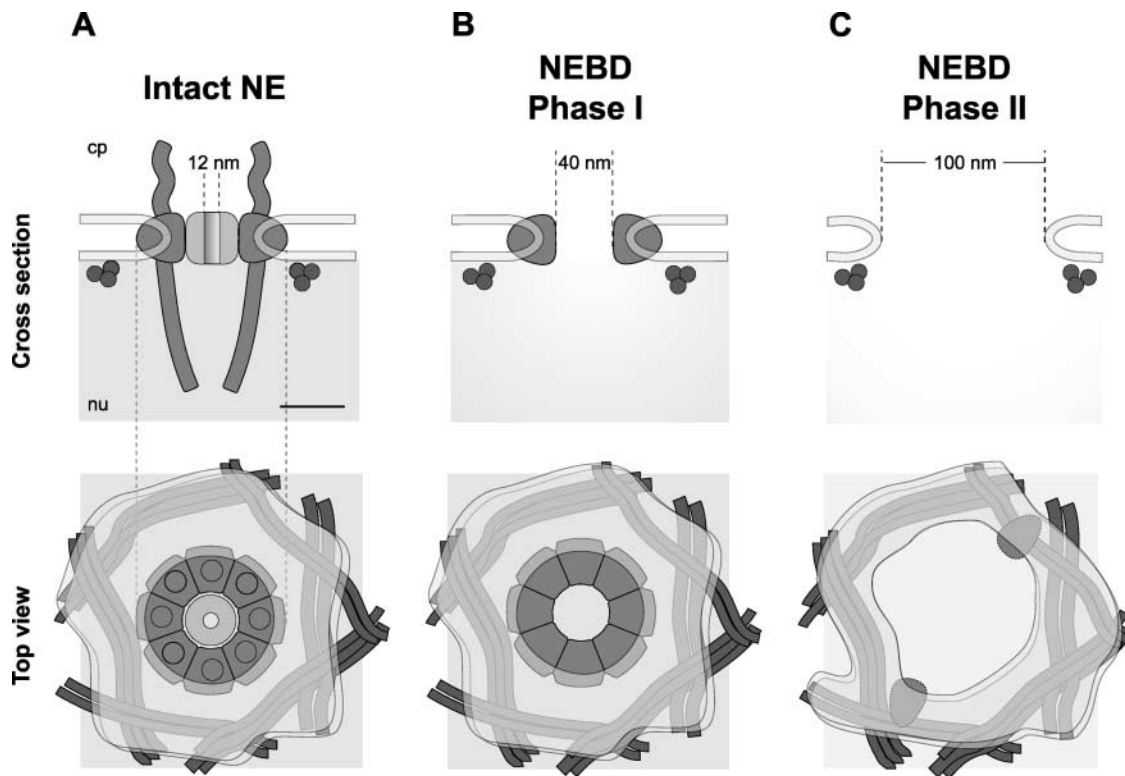


Figure 8. **Model for phase I and II of NEBD.** (Top) cross section of the NE through the center of an NPC. (Bottom) top view from the cytoplasmic side of the NE. Lamina, dark gray; nuclear membranes, transparent gray; NPC, middle gray; permeability barrier of NPC, light gray. The channel diameter indicated by dashed lines corresponds to the apparent diffusion channel calculated from dextran fluxes. (A) immature oocytes, (B) phase I oocytes, (C) phase II oocytes. Bar, 50 nm.

discontinuities in the NE, which would have allowed all dextrans to enter the nucleus simultaneously independent of their size (Fig. S1). The different entry times cannot be explained by the different diffusion coefficients of the dextrans, as evidenced by the very similar rates of entry once a given size was allowed to pass the NPC.

(b) Peripheral nucleoporins dissociated from the nuclear rim coinciding with the release of import substrates. Similar to the dextrans, this process was sequential, dissociation of different proteins started at different times, well correlated with the increase in permeability. The release was homogeneous all along the rim, again arguing against local disassembly. In the limited set of nucleoporins we studied, Nup98 and Nup153, components of the nuclear basket (Radu et al., 1995; Walther et al., 2001), were released first, followed by Nup214/CAN on the cytoplasmic face of the channel (Walther et al., 2002). POM121, a stable component of the NPC core complex (Hallberg et al., 1993; Daigle et al., 2001), was not released, suggesting that the core of NPCs remained intact. In addition, the dissociation of nucleoporins was accompanied by a gradual release of import substrates, in contrast to a massive release expected from the complete removal of NPCs as it occurs in case of viral disruptions of the NE (de Noronha et al., 2001). Furthermore, the number and length of cytoplasmic and nuclear filaments detected by EM was reduced, while core NPCs appeared intact throughout phase I.

(c) The size of the diffusion channel dilated from 10 to 40 nm. The molecular flux measurements of dextrans during phase I allowed us to calculate the size of the diffusion channel in each NPC, assuming that all $\sim 10^6$ NPCs behave in a similar manner (Table I; Online supplemental material). Strikingly, the calculated channel sizes are in good agreement with the known physical dimensions of NPCs, strongly suggesting that most pores do indeed change their permeability properties at the same time. In immature oocytes the fluxes predicted a diffusion channel diameter of ~ 12 nm, close to values measured earlier in *Xenopus* oocytes (Paine et al., 1975) and *Xenopus* NEs in vitro (Keminer and Peters, 1999). The peak fluxes at the end of phase I of NEBD predicted an ~ 40 -nm diameter, perfectly consistent with an “empty” spoke ring complex (Hinshaw et al., 1992; Akey and Radermacher, 1993) and in good agreement with the size of the largest particles that can be transported through NPCs (Pante and Kann, 2002). Even if NPCs were to dilate to 50 nm, the largest possible diameter that could still exclude the 160-kD dextran, at least 50,000 pores would have to be partially disassembled to support the observed fluxes at the end of phase I. Importantly, NPC intermediates similar to empty spoke ring complexes have recently been observed in *Drosophila* embryos during NEBD by scanning EM (Kiseleva et al., 2001).

(d) NE structure in general was unaffected during phase I. The model that only part of the NPC is disassembled during phase I is demonstrated by the ability of the NE to still exclude dextrans larger than the inner diameter of the spoke ring complex (160 kD), the unchanged concentration of core nucleoporins as well as B type lamins on the rim and the absence of gaps in the NE either by fluorescence, DIC, or at the ultrastructural level.

The gradual disassembly of NPCs at the start of NEBD

has implications for the regulation of oocyte maturation. MPF, one of the key kinases in this process, accumulates in the nucleus shortly after its activation (Ookata et al., 1992). In starfish, this accumulation starts during phase I of NEBD when NPCs begin to disassemble (unpublished data), consistent with the notion that nucleoporin release is triggered by MPF phosphorylation. Nuclear accumulation of MPF would thus at the same time alter the nuclear transport machinery and thereby change its own entry rate. Such a feedback loop could be part of the regulation of the G2/M transition, by enhancing MPF's autoamplification (Ferrell, 1998). This idea is further supported by the fact that blocking nuclear transport by a dominant negative form of importin- β (Kutay et al., 1997) prevents oocyte maturation (Fig. S5).

The nucleocytoplasmic boundary is disrupted by local removal of NPCs

Phase II of NEBD, which had a duration of only 30–40 s, allowed the rapid entry of the 500-kD dextran with a diameter of 93 nm similarly to YOYO-1-stained structures, presumably representing ribosomes (Terasaki, 1994). Particles of this size would not be able to pass through an intact core NPC channel, especially not with kinetics close to free diffusion. Indeed, by EM the zone of permeabilization consisted of NE fragments containing 3–10 NPCs separated by 100–200-nm gaps. Larger gaps were not detected by EM at this time, and the lamina and the nuclear membranes remained intact at the resolution of the confocal microscope, in agreement with earlier EM studies that reported that the lamina still forms a continuous mesh with openings of 100–150 nm at this stage of oocyte maturation (Stricker and Schatten, 1989). Although we could not resolve the formation of the gaps by live cell imaging due to the tight packing of pore complexes, based on our ultrastructural data we propose that phase II represents the rapid removal of whole NPCs from the NE. This would cause the first large perforations in the nuclear membranes, the size of which would only be limited by the persisting attachment of the membranes to the underlying lamina mesh (Fig. 8 C).

Complete permeabilization of the nucleus spreads as a rapid wave across the NE

The complete permeabilization of the NE during phase II rapidly spread from a single location across the nuclear surface with a speed of $1\text{--}2 \mu\text{m s}^{-1}$. It is likely that the starting point of this wave corresponds to a single NPC. In all the oocytes we tested the initiation site was located on the animal half of the nucleus close to its equator, which could be related to the cascade of MPF activation that is believed to begin at the animal pole of oocytes (Perez-Mongiovi et al., 2000).

We can only speculate on the mechanism that propagated the permeabilization along the NE. One model would be a mechanical “domino” mechanism, in which the first break in the network of NPCs triggers its destabilization and a propagating collapse. This model is consistent with the observation that NPCs appear physically linked to each other on the ultrastructural level (Goldberg and Allen, 1996). However, our data argue against a propagated disruption of the lamina and the presence of intact pores alternated with gaps on electron

micrographs is difficult to explain by a domino mechanism. A second and not mutually exclusive model is a biochemical propagation, for example by a phosphorylation wave. A cytoplasmic kinase, such as MPF, that only slowly entered the nucleus during phase I would be able to massively diffuse into the nucleus through the first large gap. This could lead to the rapid phosphorylation-driven disassembly of the least stable neighboring NPCs, which would create new gaps, additional kinase entry and in this manner propagate the wave. It will be very interesting to investigate the spreading mechanism and its relationship to MPF activation in future studies.

NEBD in oocytes and fibroblasts

The formation of a fenestrated membrane structure as a result of NPC removal is a mechanism of NEBD distinct from the microtubule-induced tearing of the NE that gives access to large dextrans in mammalian fibroblasts (Beaudouin et al., 2002). Large gaps could not be observed at the time the wave entered the nucleus of oocytes but only appeared several minutes after complete permeabilization. Moreover, in contrast to mammalian cells (Beaudouin et al., 2002; Salina et al., 2002), removing microtubules by nocodazole had no effect on the timing or morphology of NEBD in starfish oocytes. A likely explanation for these differences is the very different cellular architecture of oocytes and fibroblasts. The volume of a starfish nucleus is $\sim 100\times$ larger and its envelope contains $\sim 500\times$ more NPCs than the nucleus of a typical fibroblast. In contrast, the size of chromosomes and microtubule asters is very similar between oocytes and somatic cells. Thus, in oocytes, the spindle microtubules are short compared with the nucleus and can probably not generate the forces necessary to tear the lamina of the giant NE.

If one disregards the contribution of microtubules in fibroblasts, there are nevertheless similarities between both cell types. In both systems, lamina disassembly occurs long after disrupting the nucleocytoplasmic boundary. Moreover similar to starfish oocytes, an increase in NE permeability for smaller dextrans before tearing can also be observed in mammalian cells (unpublished data). Thus, starfish oocytes likely represent a good system to observe the effects of MPF activation on nuclear structure without the additional mechanical effects generated by the mitotic spindle in somatic cells.

Materials and methods

Oocyte injection and maturation

Starfish (*Asterina miniata*) were obtained from Marinus, Inc. and kept in natural seawater (Biologische Anstalt Helgoland) in aquariums at 15°C. Oocytes were isolated as described in (Terasaki, 1994), mounted into chambers and injected with mercury filled needles using methods described elsewhere (Hiramoto, 1962; Kiehart, 1982; Terasaki and Jaffe, 1993; <http://egg.uchc.edu/panda/injection/index.html>). Injection and microscopy was done at 20°C. Unless indicated otherwise, oocytes were incubated for at least 30 min after injection to allow fluorescent markers to distribute homogeneously. mRNA injected oocytes were incubated overnight or in case of low expression for 36 h at 16°C to obtain sufficient translation. Maturation was triggered by addition of 2–5 μM 1-methyladenine (Sigma-Aldrich). Phase II of NEBD typically started 20 min after hormone addition and only oocytes starting between 15–35 min were analyzed.

Fluorescent dextrans

Different sized dextran fractions were purchased either already in fluorescently labeled form (10, 70, 160 kD) or as amino derivatives (25, 90, and 500 kD) (for suppliers see Table S1). The latter were labeled with Alexa

488 (succinimidyl ester; Molecular Probes) or Cy5 (fluorolink Ab-labeling kit; Amersham Biosciences). Free dye was removed by a Nanosep 30K Omega spin column (Pall Gelman). Dextrans were dissolved in water and the concentrations of the stock solutions were determined by anthrone reaction (Luby-Phelps, 1989). Fluorescence correlation spectroscopy measurements were performed on a ZEISS LSM510 confocal microscope equipped with ConfoCor 2 FCS device (Carl Zeiss MicroImaging, Inc.) (for detailed description see Online supplemental material available at <http://www.jcb.org/cgi/content/full/jcb.200211076/DC1>). Calculated diffusion coefficients are shown in Table I. Oocytes were injected typically with a mixture of three different dextrans to 1% of the egg volume; in case only a single dextran was injected its amount was reduced to keep a similar cytoplasmic concentration.

GFP constructs and fluorescent markers

All constructs were initially cloned into mammalian expression backbones containing EGFP (CLONTECH Laboratories, Inc.) and subsequently subcloned to pGEMHE (Liman et al., 1992) for in vitro transcription (for detailed description see Online supplemental material). From linearized templates, capped mRNA was synthesized using the mMessage mMachine kit (Ambion). DiI_{C16}(3) (Molecular Probes) was dissolved in household vegetable oil to saturation and injected into oocytes (Terasaki, 1994). Alexa 488-labeled MBP and Alexa 594 IBB-MBP and M9-MBP was a gift from Katharina Ribbeck (EMBL, Heidelberg, Germany). From the concentrated stocks (270, 100, and 100 μM , respectively), amounts corresponding to 1% of the egg volume were injected.

Confocal microscopy and image quantitation

Imaging was done on a customized ZEISS LSM510 Axiovert confocal microscope as described previously (Daigle et al., 2001; Gerlich et al., 2001) using a 40 \times C-Apochromat 1.2 NA water immersion objective lens (Carl Zeiss MicroImaging, Inc.). Some experiments were also performed on a Nikon C1 E-800 confocal microscope using a 20 \times SuperFluar 0.7 NA dry lens (Nikon). Time series were analyzed in the LSM510 software (Carl Zeiss MicroImaging, Inc.), ImageJ (<http://rsb.info.nih.gov/ij/>), and NIH image (<http://rsb.info.nih.gov/nih-image/>). For further details on the imaging system and data analysis see Online supplemental material. Figures were assembled in Adobe Photoshop and Adobe Illustrator (Adobe Systems, Inc.).

Electron microscopy

Oocytes were fixed every 2 min after hormone addition and the point of NEBD was determined by following oocytes at the same time by transmitted light microscopy. They were fixed in 1% glutaraldehyde in sea water for 2 h, rinsed in sea water, and stored at 4°C. Then they were embedded in agarose and postfixed for 1 h with 1% OsO₄ and 0.8% potassium ferricyanide in cacodylate buffer, rinsed thoroughly in distilled water, and stained in 0.5% aqueous uranyl acetate for 1 h. They were dehydrated in ethanol and embedded in Poly/Bed resin (Polysciences). Ultrathin sections were stained with uranyl acetate and lead citrate and examined in a transmission electron microscope (CM-10 and BioTwinII; Philips).

Online supplemental material

The online version of this paper contains supplemental videos for Figs. 1, 2, and 4–7, as well as a detailed description of GFP constructs, imaging methods, and characterization of dextran fractions. Online supplemental material can be found at <http://www.jcb.org/cgi/content/full/jcb.200211076/DC1>.

The authors would like to acknowledge Joël Beaudouin for help with the dextran analysis and Katharina Ribbeck for fruitful discussions. We thank Katharina Ribbeck and Dirk Görlich for providing fluorescently labeled MBP, IBB-MBP, and M9-MBP; Elisa Izaurrealde for providing the Nup98 cDNA; and Maarten Fornerod for providing the Nup214 cDNA. We thank Elisa Izaurrealde and Iain Mattaj for critical reading of the manuscript.

Part of this work was performed at the Marine Biological Laboratory (MBL) in Woods Hole, MA, supported by a summer research fellowship of Nikon Inc., USA, to J. Ellenberg. J. Ellenberg also acknowledges support by the Human Frontiers Science Program (RGP0031/2001-M). P. Lenart was supported by a predoctoral fellowship of the Louis-Jeantet Foundation, Geneva, Switzerland. G. Rabut was supported by a fellowship through EMBL's international Ph.D. Programme.

Submitted: 18 November 2002

Revised: 7 February 2003

Accepted: 14 February 2003

References

- Akey, C.W., and M. Radermacher. 1993. Architecture of the *Xenopus* nuclear pore complex revealed by three-dimensional cryo-electron microscopy. *J. Cell Biol.* 122:1–19.
- Allen, T.D., J.M. Cronshaw, S. Bagley, E. Kiseleva, and M.W. Goldberg. 2000. The nuclear pore complex: mediator of translocation between nucleus and cytoplasm. *J. Cell Sci.* 113(Pt 10):1651–1659.
- Beaudouin, J., D. Gerlich, N. Daigle, R. Eils, and J. Ellenberg. 2002. Nuclear envelope breakdown proceeds by microtubule-induced tearing of the lamina. *Cell.* 108:83–96.
- Brejck, K., T.K. Sixma, P.A. Kitts, S.R. Kain, R.Y. Tsien, M. Ormo, and S.J. Remington. 1997. Structural basis for dual excitation and photoisomerization of the *Aequorea victoria* green fluorescent protein. *Proc. Natl. Acad. Sci. USA.* 94:2306–2311.
- Burke, B., and J. Ellenberg. 2002. Remodelling the walls of the nucleus. *Nat. Rev. Mol. Cell Biol.* 3:487–497.
- Burke, B., and C.L. Stewart. 2002. Life at the edge: the nuclear envelope and human disease. *Nat. Rev. Mol. Cell Biol.* 3:575–585.
- Collas, P. 1999. Sequential PKC- and Cdc2-mediated phosphorylation events elicit zebrafish nuclear envelope disassembly. *J. Cell Sci.* 112(Pt 6):977–987.
- Cronshaw, J.M., A.N. Krutchinsky, W. Zhang, B.T. Chait, and M.J. Matunis. 2002. Proteomic analysis of the mammalian nuclear pore complex. *J. Cell Biol.* 158:915–927.
- Daigle, N., J. Beaudouin, L. Hartnell, G. Imreh, E. Hallberg, J. Lippincott-Schwartz, and J. Ellenberg. 2001. Nuclear pore complexes form immobile networks and have a very low turnover in live mammalian cells. *J. Cell Biol.* 154:71–84.
- de Noronha, C.M., M.P. Sherman, H.W. Lin, M.V. Cavois, R.D. Moir, R.D. Goldman, and W.C. Greene. 2001. Dynamic disruptions in nuclear envelope architecture and integrity induced by HIV-1 Vpr. *Science.* 294:1105–1108.
- Draviam, V.M., S. Orrechia, M. Lowe, R. Pardi, and J. Pines. 2001. The localization of human cyclins B1 and B2 determines CDK1 substrate specificity and neither enzyme requires MEK to disassemble the Golgi apparatus. *J. Cell Biol.* 152:945–958.
- Ellenberg, J., E.D. Siggia, J.E. Moreira, C.L. Smith, J.F. Presley, H.J. Worman, and J. Lippincott-Schwartz. 1997. Nuclear membrane dynamics and reassembly in living cells: targeting of an inner nuclear membrane protein in interphase and mitosis. *J. Cell Biol.* 138:1193–1206.
- Ferrell, J.E., Jr. 1998. How regulated protein translocation can produce switch-like responses. *Trends Biochem. Sci.* 23:461–465.
- Gerace, L., and G. Blobel. 1980. The nuclear envelope lamina is reversibly depolymerized during mitosis. *Cell.* 19:277–287.
- Gerace, L., and B. Burke. 1988. Functional organization of the nuclear envelope. *Annu. Rev. Cell Biol.* 4:335–374.
- Gerlich, D., J. Beaudouin, M. Gebhard, J. Ellenberg, and R. Eils. 2001. Four-dimensional imaging and quantitative reconstruction to analyse complex spatiotemporal processes in live cells. *Nat. Cell Biol.* 3:852–855.
- Goldberg, M.W., and T.D. Allen. 1996. The nuclear pore complex and lamina: three-dimensional structures and interactions determined by field emission in-lens scanning electron microscopy. *J. Mol. Biol.* 257:848–865.
- Görlich, D., and U. Kutay. 1999. Transport between the cell nucleus and the cytoplasm. *Annu. Rev. Cell Dev. Biol.* 15:607–660.
- Gruenbaum, Y., K.L. Wilson, A. Harel, M. Goldberg, and M. Cohen. 2000. Review: nuclear lamins—structural proteins with fundamental functions. *J. Struct. Biol.* 129:313–323.
- Hallberg, E., R.W. Wozniak, and G. Blobel. 1993. An integral membrane protein of the pore membrane domain of the nuclear envelope contains a nucleoporin-like region. *J. Cell Biol.* 122:513–521.
- Hinshaw, J.E., B.O. Carragher, and R.A. Milligan. 1992. Architecture and design of the nuclear pore complex. *Cell.* 69:1133–1141.
- Hiramoto, Y. 1962. Microinjection of live spermatozoa into sea urchin eggs. *Exp. Cell Res.* 27:416–426.
- Keminer, O., and R. Peters. 1999. Permeability of single nuclear pores. *Biophys. J.* 77:217–228.
- Kiehart, D.P. 1982. Microinjection of echinoderm eggs: apparatus and procedures. *Methods Cell Biol.* 25:13–31.
- Kiseleva, E., S. Rutherford, L.M. Cotter, T.D. Allen, and M.W. Goldberg. 2001. Steps of nuclear pore complex disassembly and reassembly during mitosis in early *Drosophila* embryos. *J. Cell Sci.* 114:3607–3618.
- Kishimoto, T. 1999. Activation of MPF at meiosis reinitiation in starfish oocytes. *Dev. Biol.* 214:1–8.
- Kohler, R.H., P. Schwille, W.W. Webb, and M.R. Hanson. 2000. Active protein transport through plastid tubules: velocity quantified by fluorescence correlation spectroscopy. *J. Cell Sci.* 113:3921–3930.
- Kutay, U., E. Izaurralde, F.R. Bischoff, I.W. Mattaj, and D. Görlich. 1997. Dominant-negative mutants of importin-beta block multiple pathways of import and export through the nuclear pore complex. *EMBO J.* 16:1153–1163.
- Liman, E.R., J. Tytgat, and P. Hess. 1992. Subunit stoichiometry of a mammalian K⁺ channel determined by construction of multimeric cDNAs. *Neuron.* 9:861–871.
- Luby-Phelps, K. 1989. Preparation of fluorescently labeled dextrans and ficolls. *Methods Cell Biol.* 29:59–73.
- Marshall, I.C.B., and K.L. Wilson. 1997. Nuclear envelope assembly after mitosis. *Trends Cell Biol.* 7:69–74.
- Nigg, E.A. 1992. Assembly-disassembly of the nuclear lamina. *Curr. Opin. Cell Biol.* 4:105–109.
- Ookata, K., S. Hisanaga, T. Okano, K. Tachibana, and T. Kishimoto. 1992. Relocation and distinct subcellular localization of p34cdc2-cyclin B complex at meiosis reinitiation in starfish oocytes. *EMBO J.* 11:1763–1772.
- Paine, P.L., L.C. Moore, and S.B. Horowitz. 1975. Nuclear envelope permeability. *Nature.* 254:109–114.
- Pante, N., and U. Aebi. 1996. Toward the molecular dissection of protein import into nuclei. *Curr. Opin. Cell Biol.* 8:397–406.
- Pante, N., and M. Kann. 2002. Nuclear pore complex is able to transport macromolecules with diameters of about 39 nm. *Mol. Biol. Cell.* 13:425–434.
- Perez-Mongiovi, D., C. Beckhelling, P. Chang, C.C. Ford, and E. Houlston. 2000. Nuclei and microtubule asters stimulate maturation/M phase promoting factor (MPF) activation in *Xenopus* eggs and egg cytoplasmic extracts. *J. Cell Biol.* 150:963–974.
- Radu, A., M.S. Moore, and G. Blobel. 1995. The peptide repeat domain of nucleoporin Nup98 functions as a docking site in transport across the nuclear pore complex. *Cell.* 81:215–222.
- Ribbeck, K., and D. Görlich. 2001. Kinetic analysis of translocation through nuclear pore complexes. *EMBO J.* 20:1320–1330.
- Ribbeck, K., and D. Görlich. 2002. The permeability barrier of nuclear pore complexes appears to operate via hydrophobic exclusion. *EMBO J.* 21:2664–2671.
- Rout, M.P., J.D. Aitchison, A. Suprapto, K. Hjertaas, Y. Zhao, and B.T. Chait. 2000. The yeast nuclear pore complex: composition, architecture, and transport mechanism. *J. Cell Biol.* 148:635–651.
- Salina, D., K. Bodoor, D.M. Eckley, T.A. Schroer, J.B. Rattner, and B. Burke. 2002. Cytoplasmic dynein as a facilitator of nuclear envelope breakdown. *Cell.* 108:97–107.
- Spurlino, J.C., G.Y. Lu, and F.A. Quioco. 1991. The 2.3-A resolution structure of the maltose- or maltodextrin-binding protein, a primary receptor of bacterial active transport and chemotaxis. *J. Biol. Chem.* 266:5202–5219.
- Stricker, S.A., and G. Schatten. 1989. Nuclear envelope disassembly and nuclear lamina depolymerization during germinal vesicle breakdown in starfish. *Dev. Biol.* 135:87–98.
- Stricker, S.A., and G. Schatten. 1991. The cytoskeleton and nuclear disassembly during germinal vesicle breakdown in starfish oocytes. *Develop. Growth and Differ.* 33:163–171.
- Terasaki, M. 1994. Redistribution of cytoplasmic components during germinal vesicle breakdown in starfish oocytes. *J. Cell Sci.* 107(Pt 7):1797–1805.
- Terasaki, M., P. Campagnola, M.M. Rolls, P.A. Stein, J. Ellenberg, B. Hinkle, and B. Slepchenko. 2001. A new model for nuclear envelope breakdown. *Mol. Biol. Cell.* 12:503–510.
- Terasaki, M., and L.A. Jaffe. 1993. Imaging of the endoplasmic reticulum in living marine eggs. In *Cell Biological Applications of Confocal Microscopy*. Vol. 38. B. Matsumoto, editor. Academic Press, Orlando, FL. 211–220.
- Vigers, G.P., and M.J. Lohka. 1991. A distinct vesicle population targets membranes and pore complexes to the nuclear envelope in *Xenopus* eggs. *J. Cell Biol.* 112:545–556.
- Walther, T.C., M. Fornerod, H. Pickersgill, M. Goldberg, T.D. Allen, and I.W. Mattaj. 2001. The nucleoporin Nup153 is required for nuclear pore basket formation, nuclear pore complex anchoring and import of a subset of nuclear proteins. *EMBO J.* 20:5703–5714.
- Walther, T.C., H.S. Pickersgill, V.C. Cordes, M.W. Goldberg, T.D. Allen, I.W. Mattaj, and M. Fornerod. 2002. The cytoplasmic filaments of the nuclear pore complex are dispensable for selective nuclear protein import. *J. Cell Biol.* 158:63–77.
- Worman, H.J., and J.C. Courvalin. 2000. The inner nuclear membrane. *J. Membr. Biol.* 177:1–11.
- Yang, L., T. Guan, and L. Gerace. 1997. Integral membrane proteins of the nuclear envelope are dispersed throughout the endoplasmic reticulum during mitosis. *J. Cell Biol.* 137:1199–1210.